Available online at www.sciencedirect.com

ScienceDirect

journal homepage: www.elsevier.com/locate/he

Synthesis and characterization of MWCNT incorporated N, S-rGO supported CdS photocatalyst for the dissociation of water to hydrogen by visible light

*Zahoor Alam, Bhawna Verma, A.S.K. Sinha**

Department of Chemical Engineering and Technology, IIT (BHU), Varanasi, India

HIGHLIGHTS

- Reported preparation method promotes chemical interaction between CdS and N,S-rGO.
- Interaction facilitates a quick transfer of electrons for the reduction of H_2O.
- Incorporation of MWCNT prevents re-stacking of N,S-rGO layers.
- MWCNT enhances light absorption, charge carriers and electrical conductivity.
- The synergetic effect of MWCNT on N, S-rGO results a better activity.

GRAPHICAL ABSTRACT

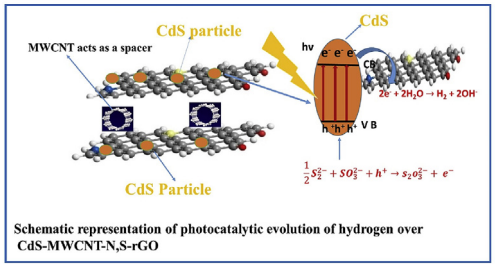

Schematic representation of photocatalytic evolution of hydrogen over CdS-MWCNT-N,S-rGO

ARTICLE INFO

Article history:
Received 8 August 2019
Received in revised form
12 October 2019
Accepted 24 October 2019
Available online 15 November 2019

Keywords:
MWCNT
Restacking
Chemical interaction
Solar hydrogen

ABSTRACT

In the present study, MWCNT-N,S-rGO supported CdS was synthesized at a higher temperature by the gas-solid reaction. Photoactivity was measured and compared with N, S-rGO supported CdS. Incorporation of MWCNT prevents the restacking of the graphene layer and provides the high surface area for the dispersion of CdS which result in increasing the photoactivity of catalyst. It also increases the electrical conductivity which reduces the charge transfer resistance. Catalysts were characterized by FTIR, XRD, XPS, Raman spectroscopy, BET surface area analyzer, TEM, HRTEM, UV–Vis spectroscopy, PL spectroscopy, electrochemical impedance spectroscopy (EIS) and Mott. Schottky analysis. The characterization results confirmed that incorporating MWCNT in N,S- rGO resulted in a higher rate of electron generation and also a higher rate of transfer of electrons to the solid-liquid interface and hence a higher activity.

* *Corresponding author.*
E-mail address: asksinha.che@itbhu.ac.in (A.S.K. Sinha).

https://doi.org/10.1016/j.ijhydene.2019.10.183

Introduction

Worldwide, the demand for renewable energy has been proliferating to suppress the environment pollution and become an alternative of fossil fuels. Photocatalytic generation of H_2 from water using solar light is a promising way to harness renewable energy. To achieve this goal, there is a need for highly efficient and imperishable visible light-driven photocatalysts. Extensive work carried out in the past few decades has resulted into the development of several photocatalysts. Among them, Cadmium sulfide (CdS) is a very fascinating photocatalyst because of its narrow band gap (2.42 eV) and its conduction band minimum is more negative than the reduction potential of H_2O to H_2 [1,2]. Nevertheless, photocatalytic application of CdS is limited because of quick recombination of photoinduced electrons and holes. For preventing the recombination of electrons and holes of CdS, several authors have applied a number of strategies such as noble-metal loading [3–5], constructing binary [6–8] and ternary hybrid photocatalysts and developing heterojunction between them for transfer of electrons [9,10]. Moreover, fast electrons mobility of photocatalysts enhanced the photoactivity by preventing the charge recombination. In this context, graphene a carbonaceous material has attracted the attention of the researchers in the field of photocatalysis because graphene has two-dimensional (2D) structure of sp2 hybridized carbon atoms, excellent electrical conductivity and high surface area [11,12]. Furthermore, oxidised and exfoliated graphene has functional groups present on the surface of graphene which may develop chemical interaction with other species leading to the formation of heterojunction [13]. For the utilization of the aforementioned characteristic properties of graphene, several authors have synthesized rGO supported CdS by using the most commonly hydrothermal/solvothermal technique and reported a hydrogen production activity by the photocatalytic splitting of water. There are further reports in the literature where authors have developed heteroatoms (N. P, B, S) -doped graphene oxide to tailor the optical and electrical properties of graphene oxide [14–18]. Doping of heteroatoms into graphene oxide could increase the electrical conductivity because such atoms contribute extra P electrons to the π system of graphene [19,20]. Jia et al. [21] have synthesized N-graphene/CdS by calcination and they reported that N-rGO/CdS exhibits a higher hydrogen production due to the development of heterojunction between N-rGO and CdS. They also explained that N-rGO acts as a charge collector and facilitate the transfer of electrons and thus prevent the recombination of photoinduced charge within CdS. Kon et al. [22] have reported that graphitic carbon nitrides have remarkable catalytic properties. Han et al. [23] have also reported that CdS supported on the surface of N-rGO showed better activity than bare CdS. Weiwei Han et al. [24] have synthesized CdS/N,S-rGO nanocomposite and reported a superior activity than CdS/rGO because the incorporation of N,S-rGO reduced the band-gap and also increased the absorption of light. It is also reported that in r GO and GO re-stacking of layers occurs, mostly at the preparation stage of reduction and doping, due to the stacking of layers in graphene because of the presence of π-π interaction and strong Van der Wall force of attraction. The re-stacking reduces the electrical conductivity and surface area of rGO or doped rGO [25]. A few works have been reported to overcome the aforementioned problem of re-stacking by intercalation of CNT into graphene because CNT has 1D nano cylindrical structure and high electrical conductivity [26–28]. Recently, multi-walled carbon nanotube (MWCNT) supported catalysts have been studied for photocatalysis owing to high electrical conductivity, a higher specific surface area providing an electron transfer channel and also for having a light-harvesting property [9,29–31]. It has also been widely used as a spacer to prevent the stacking of graphene oxide. For example, Robel et al. [32] reported that single-wall carbon nanotube (SWCNT) supported CdS showed that photogenerated electrons were quickly transferred from the CdS to SWCNT. Peng et al. [33] synthesized CdS supported MWCNT by a hydrothermal technique and reported that the presence MWCNT enhanced the activity as it had a higher electrical conductivity facilitate the transfer of photogenerated electrons from the CdS to the surface of the MWCNT. Shen et al. [34] have also synthesized CNT intercalated graphene supported TiO_2 and found that CNT restored the conductivity and maximised the surface area of graphene. Furthermore, Wan- Kuen Jo and Selvam synthesized ternary CdS/MoS_2/MWCNT by a hydrothermal method and reported a better photoactivity. Arvind and Sinha [35] synthesized a composite of CdS/rGO by a solid-gas reaction method and illustrated the existence of a chemical interaction at the interface of CdS and graphene and reported that the catalyst was more active compared to one prepared by the hydrothermal synthesis. They concluded that the chemical interaction had resulted into formation of a heterojunction which facilitated a rapid movement of electrons from the conduction band of CdS to rGO.

In the present study, we have synthesized MWCNT incorporated N,S-rGO supported CdS photocatalyst. Objectives were to prevent re-stacking of rGO sheet and also to have higher surface area for a better photocatalyst activity. In addition, the inclusion of MWCNT was considered to promote charge transfer from CdS. A gas-solid reaction method for catalyst preparation was selected to promote the formation of heterojunction for charge separation. The superior activity of the catalyst has been explained by analysing the microstructure of the catalyst.

Experimental

Catalyst preparation

Synthesis of Graphite oxide (GO) Graphite oxide was prepared by adopting the Hummers' method. 1.0 g of $NaNO_3$ and 2.0 g of graphite powder was added into the beaker and the temperature of beaker maintained below 283 K by an ice bath. Subsequently, 98 mL of H_2SO_4 was added and stirred for an hour to make the complete dispersion of $NaNO_3$ and graphite powder. 6.0 g of $KMnO_4$ was gradually added in the suspension with constant stirring. The mixture was constantly stirred for an hour. The mixture was then put on the hot plate for 30 min at 308 K. As the reaction progressed, the mixture gradually thickened. 100 mL of double-distilled water was slowly added

to the reaction mixture and it was stirred for 30 min at 371 K. After 30 min, again 180 mL of double distilled water was again added followed by adding 30% H_2O_2 to neutralise the unreacted potassium permanganate. The obtained product was centrifuged at 6000 rpm. Products obtained from centrifuge was rinsed with 5% of the HCl solution to remove the impurities (Fe, Mn etc) and subsequently was rinsed with double distilled water several times to remove the sulphate ions. Finally. barium chloride test was performed and no white precipitate of barium sulphate was detected. In the end, the obtained cake of GO was dried in a vacuum oven for overnight at 342 K.

Synthesis of N,S-rGO: 450.0 mg of GO powder was taken and dissolved into 150 mL of double distilled water and sonicated for 2 h to exfoliate the GO sheet and subsequently, 3.0 g of thiourea (NH_2CSNH_2) was added and stirred for 2 h to make the mixture homogenous. After that, the mixture was poured into 200 mL Teflon lined autoclave which was heated at 463 K for 12 h. The obtained product was rinsed with double distilled water. Further, it was dried in a hot air oven at 343 K for 12 h.

Synthesis of MWCNT-N,S-rGO: 300 mg multi-walled carbon nanotube (MWCNT), procured from Sisco Research Laboratories Pvt Ltd., was added to 100 mL of dilute HCl solution (2 M) and stirred for more than 5 h; followed by sonication using ultra probe sonicator. It was subsequently centrifuged and rinsed with distilled water to remove the metallic impurities. 100 mg of pre-treated MWCNT powder (10 wt% of N,S-rGO) was subsequently added to 1.0 g of N,S-rGO dispersed in double-distilled water and sonicated for 4 h by using ultra probe sonicator to make high dispersion of N,S-rGO and MWCNT in distilled water. High power sonication was applied because MWCNT powder has a hydrophobic nature. The mixture was autoclaved at 463 K for 6 h. The resulting product was then rinsed with distilled water and dried in a hot air oven at 343 K for 12 h.

Catalyst-1: It was N,S-rGO supported CdS prepared by the gas-solid reaction method. The weight ratio of CdS to N,S-rGO was 1: 2. The required amount of N,S-rGO was taken and added in a dilute aqueous solution of $CdSO_4$. The mixture was dried on a water bath at 383 K with mechanical stirring. Subsequently, the dried mass was put in a hot air oven at 373 K for 12 h. The solid mass was made into granules. These dried granules were placed into a quartz tubular reactor and purged with N_2 gas to remove the air to prevent the conversion $CdSO_4$ to CdO. Subsequently, H_2S gas was passed into the tubular reactor at 573 K for 4 h which reacted with $CdSO_4$ to form CdS.

Catalyst-2: MWCNT incorporated N,S-rGO supported CdS (CdS-MWCNT-N,S-rGO) was prepared by following the same preparation protocol of catalysts-1. MWCNT-N,S-rGO was used as co-catalyst in place of N,S-rGO.

Photocatalytic activity measurement

The photocatalytic reaction for H_2 generation was performed in a pyrex glass which was 250 mL flat bottom flask with three necks. Photoreactor was made of pyrex glass comprising of a flat bottomed surface. One side of photoreactor was also made into a flat vertical surface (area = 15 cm^2) for the entrance of irradiated light without much scattering. Visible light source (100 W Oriel Mercury–Xenon lamp) was used. The total volume of the reaction mixture was 250 mL which contained 1.0 g of catalyst (~200 mesh size) particles dispersed in the solution with the help of magnetic stirring. The aqueous solution was made by the addition of an equal volume of 0 0.004 M of sulphite (Na_2SO_3) and 0.01 M of sulphide (Na_2S) solutions. The pH of the aqueous solution was fixed at 8.6 by adding NaOH or CH_3COOH solution as required. Prior to light irradiation on the photoreactor, N_2 gas was purged for 1 h to remove the dissolved O_2 gas from the solution. The gas produced during the course of the experiment was collected by water displacement technique and analyzed by gas chromatography using a 10 Å carbosieve column attached with a thermal conductivity detector. The results confirmed that the gas produced was pure hydrogen. Further, the stability of the catalysts has also been performed. After the completion of the run, irradiation of light was stopped, and the reaction mixture was left for 2 h. Subsequently, N_2 gas was purged for an hour and the experiment was repeated.The same procedure was followed for repeated runs.

Catalysts characterization

The IR spectra of prepared catalysts in transmission mode were obtained in the wavenumber range of 400–4000 cm^{-1} using FTIR spectrophotometer (Nicholet 5700, Thermo Electron). Catalyst (1.0 wt % approx.) was mixed with KBr powder as an FTIR reflectance standard and made into a pellet. XRD was carried out to determine phases and mean crystallite size by using powder diffractometer (Rigaku Ultima IV) and Cu-Kα line with the wavelength of 1.542 Å was used as an X-ray source. TEM and HRTEM images were collected by using transmission electron microscopy (TechnaiG2) and it was operated at 200 kV accelerating voltage with camera length 135 mm. For the measurement of defects and layers of graphene, the catalyst was characterized using micro-Raman spectrometer (LabRAM HR, JY). Samples were excited with laser light of wavelength 632.8 nm (He–Ne laser, Spectra physics). BET surface area was measured by a Surface Area and Porosity Analyser ASAP 2020 (Micromeritics). Diffuse reflectance spectra of catalysts were collected by using UV–Vis spectrophotometer (Varian 100Bio) in the wavelength range of 800 to 400 nm $BaSO_4$ was used as the reflectance standard. To study the charge recombination of prepared catalysts, Fluorescence spectroscopy (Varian, Cary eclipse) was used to record the photoluminescence spectra (PL). X-ray photoelectron spectroscopy (AMICUS, Kratos Analytical) with MgKα line (1253.6) was used to investigate the chemical composition of synthesized catalysts. The spectral position of each peak of each sample was corrected by normalizing of C1s at 284.6 eV and peaks were deconvoluted by using Shirley background. For Mott Schottky and electrochemical impedance spectroscopy (EIS) analysis, electrodes were prepared for N, S-rGO, MWCNT-N,S-rGO and catalysts 1 and 2. 20 mg of the sample was mixed with 2 mL of N, N-dimethylformamide (Fisher Scientific) solution as dispersing medium and 50 μL of Nafion (binder) was also added and the mixture was sonicated for 2 h to have a high dispersion of catalyst particles in the DMF solution. After that, 50 μL of the dispersed catalyst was pipetted out and drop cast on the working electrode which was made of Toray carbon paper (electrode area = 0.25 cm^2)

and the electrode was allowed to dry at the room temperature. Electrical impedance measurements were carried out with a three-electrode system (μAutolab Type III). The fabricated electrode was used as the working electrode with the Pt electrode as a counter electrode and an Ag/AgCl electrode (3 M Std KCl solution) as a reference electrode. The experiment was performed at the room temperature with a frequency range from 100 kHz to 0.1 Hz at an applied potential of 100 mV (RMS) as an amplitude of ac frequency. All the experiments were carried out in open circuit potential. 10 data points were recorded per decades of frequency. The electrolyte was an equal volume solution of 0.01 M Na_2S and 0.004 M Na_2SO_3. Mott. Schottky analyses were performed to examine flat band potential and the charge carrier density. The experiment was carried out with the same three-electrode system and the electrolyte at a frequency 10 kHz with an applied voltage of 100 mV.

Results and discussion

Activity

Photocatalytic activities of synthesized catalysts were measured in term of H_2 produced at NTP for 2 h of irradiation of visible light. Measured values are presented in Table 1. Reported values correspond to an average of a number of multiple runs. Further, no H_2 gas evolved neither in the absence of photocatalyst nor without irradiation of light. It confirmed that the following reactions were photocatalytic in nature in the process of water splitting.

$$CdS + h\upsilon \rightarrow e^-(CB) + h^+(VB) \quad (1)$$

$$2H_2O + 2e^- \rightarrow H_2 + 2OH^- \quad (2)$$

$$2h^+ + 2S^{2-} \rightarrow S_2^{2-} \quad (3)$$

$$SO_3^{2-} + S_2^{2-} \rightarrow S^{2-} + S_2O_3^{2-} \quad (4)$$

$$2h^+ + S^{2-} + SO_3^{2-} \rightarrow S_2O_3^{2-} \quad (5)$$

It can be seen from Table 1 that the photocatalytic activity of catalyst- 2 is nearly 20% higher compared to that of catalyst-1. Both catalysts 1 and 2 had the same composition of CdS and were prepared by the same preparation technique. However, it is observed that the photocatalytic activity of catalyst- 2 is nearly 20% higher compared to that of catalyst-1. The higher activity of catalyst-2 is due to the presence of multi-walled carbon nanotube (MWCNT) intercalated into N,S-rGO. MWCNT were incorporated into N,S-rGO to prevent the re-stacking of graphene layers and provide a higher surface area for the dispersion of CdS particles and increased absorption of irradiated visible light giving a higher activity. In addition, MWCNT should also increase the conductivity of the catalyst. Thus the synergistic effect of incorporation with N,S-rGO is seen to have resulted in a higher activity (catalyst 2). Moreover, the stability of catalysts was also checked by measuring activity in four repeated runs following the procedure given in section Photocatalytic activity measurement and results are reported in Table 1. It can be observed that each catalyst has shown similar rate of hydrogen production in repeated runs. It is in order to mention that the photocorrosion of CdS has been effectively prevented in the present study by the presence of sulfide and sulfite ions in the electrolyte.

FTIR spectroscopy

FTIR analysis of prepared samples was carried out to examine the functional groups. The FT-IR spectra of N,S-rGO and MWCNT intercalated N,S-rGO are shown in Fig. 1(a). Peak positions are summarized and presented in Table 2. The absorption bands at 1549 and 1440 cm^{-1} in N,S-rGO are ascribed to stretching vibration of C=C functional groups with Sp2 hybridized carbon atoms of graphene [36] and asymmetrical stretching vibration of C–N bonds [37], respectively. The band at 1190 cm^{-1}corresponds to the symmetric stretching vibration of the C–N group [38]. The peak at 950 cm^{-1} is attributed to the stretching vibration of C–C=S group [39]. On comparison MWCNT intercalated N,S-rGO shows similar bands as those appeared in N,S-rGO. Therefore, the aforementioned results confirmed the successful doping of heteroatom (N and S) has been achieved.

Fig. 1(b) represents the FTIR spectra of catalysts. Catalysts-1and 2 showed vibrational peaks which are similar to those reported in N,S-rGO and MWCNT- N,S-rGO. The exception was a peak at 630 cm^{-1} which is attributed to the stretching vibration of Cd–S [40,41]. In our previous paper [42], CdS supported N-rGO was synthesized by a solid-gas reaction at a higher temperature (573 K) which had resulted in the formation of a –C=S functional group. This group (-C=S) is formed by the chemical interaction between π electrons of C atoms in graphene and n orbital of S atoms of CdS. It was also concluded that this chemical interaction had resulted into formation of a heterojunction at the solid-solid interface between CdS and N-rGO. Therefore, the peak appeared at 1195 cm^{-1} in catalyst-1 may also be due to the interaction of CdS and rGO because of a preparation technique involving a high temperature.

Table 1 – Catalyst activity (Vol. of H_2 gas produced in 2 h).

Catalysts	H_2 gas (mL. g-CdS^{-1})	H_2 gas (mL. g-CdS^{-1})	H_2 gas (mL. g-CdS^{-1})	H_2 gas (mL. g-CdS^{-1})
Run	1st	2nd	3rd	4th
1	16.8	16.7	16.7	16.6
2	20.4	20.4	20.3	20.2

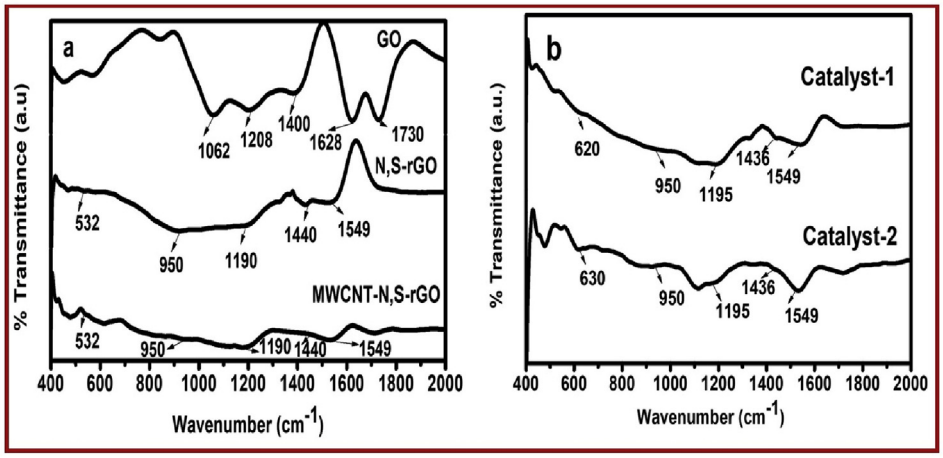

Fig. 1 – FTIR spectra (a: GO, N,S-rGO, MWCNT-N,S-rGO), (b: Catalysts 1 and 2).

Table 2 – FTIR Spectroscopy of supports and catalysts.

Functional groups	Samples			
	N,S-rGO	MWCNT-N,S-rGO	Catalyst-1	Catalyst-2
C=C graphite	1549	1549	1549	1549
Symmetric stretching of C–N	1190	1190	1190	1190
Asymmetric stretching of C–N	1440	1440	1436	1436
–C–S–C–	–	–	1195	1195
C–C=S	950	950	950	950
Cd–S stretching vibration	–	–	620	630

XRD analysis

XRD patterns of GO, N,S-rGO and MWCNT-N,S-rGO are presented in Fig. 2(a). It is observed that a sharp and intense XRD pattern of GO appeared at $2\theta = 11.95^{\circ}$ which corresponds to the (002) plane with the interplanar spacing of 7.43 Å. The increase in d -value in comparison to that of graphite (3.40 Å), indicates that in GO graphite is highly oxidised and contains various oxygen functional groups. In the case of N,S-rGO, the broad diffraction peak of (002) plane appeared at $2\theta = 24.95^{\circ}$ with the interplanar spacing of 3.57 Å. N,S-rGO had still a higher d-value than graphite after doping and reduction because of two reasons. Firstly, some intercalated H_2O molecules may be present between the layers of N,S-rGO. Secondly, the atomic size of S atom (1.09 Å) is greater than that of C (0.77 Å) and has formed the C–S–C group at the basal plane of N,S-rGO. This functional group was confirmed by analysis of FTIR spectra of N,S-rGO. In comparison to NS-rGO, MWCNT-N,S-rGO exhibits lower diffraction angle $2\theta = 24.54^{\circ}$ for (002) plane and its interplanar spacing was increased d = 3.63 Å.

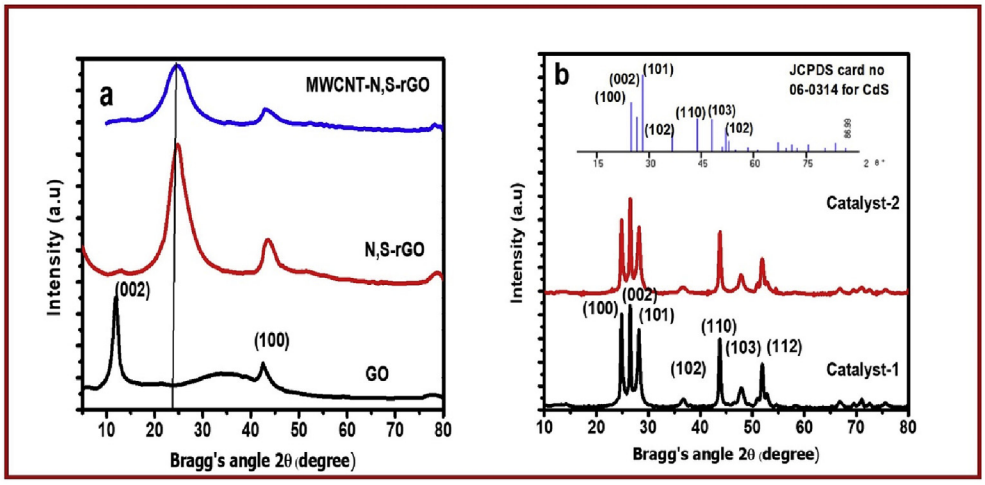

Fig. 2 – XRD patterns (a: GO, N,S-rGO, MWNT-N,S-rGO), (b: catalysts 1 and 2).

The increased in d-value is due to the hybridization of MWCNT with N,S-rGO. MWCNT has 1D nano cylindrical structure and π conjugation. This π conjugation interacts with the π conjugation of N,S-rGO and holds the MWCNT between the layer of N, S-rGO. This result indicates that MWCNT is intercalated between the layer of N,S-rGO and prevent the restacking of graphene layer during the reduction of graphite oxide (GO). Literature [43,44] also reports that when CNT is intercalated between graphene layers, d-value of graphene has increased. Aforementioned result confirmed that intercalation of MWCNT in N,S-rGO has been successfully achieved by the use of the hydrothermal technique.

XRD pattern of as-synthesized catalysts-1 to 2 are presented in Fig. 2(b). Interplanar spacings (d-value) were calculated by using Bragg's diffraction equation. Calculated values are reported in Table 3. Standard values of wurtzite structure of CdS from JCPDS file 06–0314 are also reported in Table 3. In comparison, it is found that each catalyst had a hexagonal structure of CdS. These catalysts were synthesized by a solid-gas reaction technique at high temperature. Arvind and Sinha [35] have also shown that the conversion of $CdSO_4$ to CdS in the flow of H_2S gas at high temperature (573 K) results into the hexagonal structure of CdS. It is important to note that Zhang et al. [45] demonstrates that hexagonal structure of CdS showed higher activity than the cubic phase of CdS because, in the hexagonal structure of CdS, distortion of CdS_4 tetrahedron creates an internal electric field within CdS, which favours the diffusion and separation of photoinduced charge carriers. No diffraction pattern of N,S-rGO and MWCNT-N,S-rGO for (002) plane in catalysts −1 to 2 were detected. This is due to the shielding of their peaks by the intense of CdS [21].

Unit cell parameters of the wurtzite structure of CdS were calculated using the following equation.

$$\frac{1}{d^2}=\frac{4}{3}\left[h^2+hk+\frac{k^2}{a^2}\right]+\frac{1}{c^2} \quad (6)$$

The d-values corresponding to (002) and (110) planes were used and the calculated values of the lattice parameter of wurtzite structure of CdS viz, a, c and ratio c/a are reported in Table 4. These values are similar to those reported in the literature [46]. These values confirmed that the synthesized catalysts had no defects in the structure of CdS. Furthermore, mean crystallite sizes were calculated by measuring the full width at the half intensity of (110) plane which was corrected for the instrumental broadening and the Scherrer equation was employed. The values are given in Table 4. No significant variation in the mean crystallite sizes of catalysts is observed.

TEM and HRTEM

The TEM image of MWCNT incorporated N, S-doped graphene oxide is shown in Fig. 3. It is observed from the micrograph that MWCNT is intercalated between the layer of graphene oxide and are also dispersed on the surface of graphene oxide. It is known that intercalation of MWCNT in graphene oxide would widen the distance between the layers of graphene and would also prevent the restacking of the graphene layer. The same could be concluded in the case of our samples also. HRTEM image shows highly crystalline MWCNT with an interplanar spacing of 3.48 Å corresponding to the (002) plane of MWCNT. Lattice fringes corresponding to 3.63 Å is attributed to the (002) plane of N,S-rGO in MWCNT-N,S-rGO. SAED pattern of MWCNT-N,S-rGO is presented in Fig. 3. The calculated values are 3.48 Å and 2.08 Å, which is ascribed to the (002) and (110) planes of MWCNT, respectively.

Table 3 – Results of XRD of synthesized CdS.

Standard values of interplanar spacing of CdS				Experimental values of CdS	
Hexagonal		Cubic		Hexagonal	
Miller	Hexagonal d-values	Miller indices	Cubic d- values	Catalyst-1	Catalyst-2
100	3.58	–	–	3.57	3.58
002	3.36	111	3.36	3.35	3.36
101	3.16	–	–	3.16	3.16
102	2.45	–	–	2.45	2.43
–	–	200	2.91	–	–
110	2.06	220	2.06	2.06	2.06
103	1.89	–	–	1.89	1.90
200	1.79	311	1.75	1.78	1.78
112	1.76	–	–	1.76	1.76
201	1.73	–	–	1.73	1.73
004	1.67	222	1.68	1.68	–
203	1.39	331	1.33	1.39	1.40

Table 4 – Results of lattice parameters, average crystallite size (nm) and band gap of CdS in catalysts.

Catalysts	Lattice parameters of wurtzite structure of CdS			Mean crystallite size and Particle size by		Band Gap (eV)
	a	c	c/a	XRD	TEM	
1	4.12	6.70	1.62	33	34	2.18
2	4.12	6.70	1.62	29	32	2.14

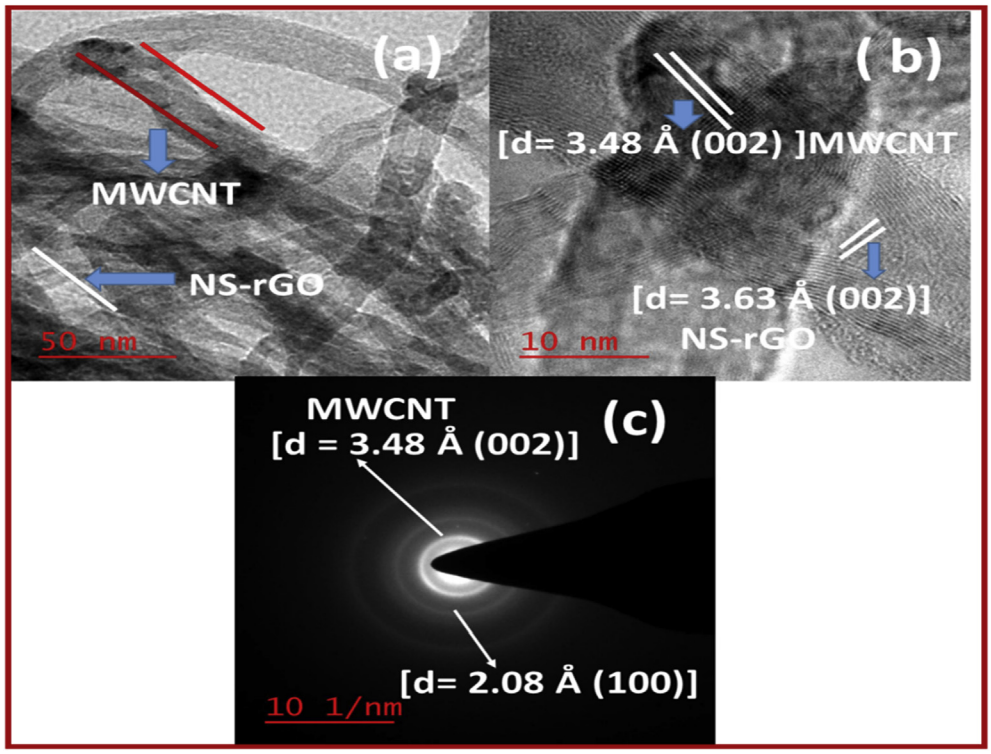

Fig. 3 – TEM image (a: MWCNT-N,S-rGO), (b: HRTEM image of MWCNT-N,S-rGO), (c: SAED patterns of MWCNT-N,S-rGO).

TEM and HRTEM micrograph of prepared catalysts-1 and 2 are presented in Fig. 4. Agglomeration of CdS particles to some extent is seen in catalysts-1 which was CdS supported on N, S-rGO. In comparison to catalyst –1, catalysts 2 shows a negligible agglomeration of CdS particles is due to the presence of MWCNT. It is seen that the MWCNT acts as a spacer and has prevented agglomeration of CdS particles. Thus, the MWCNT not only facilitated dispersion of CdS particle on the

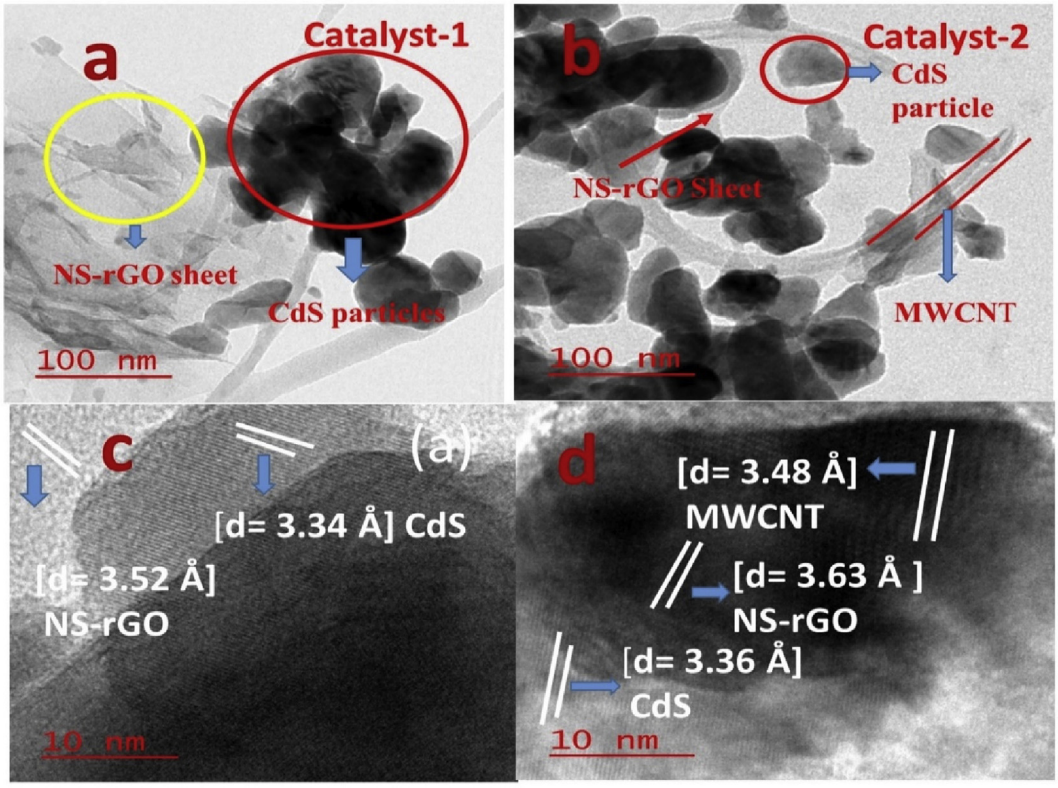

Fig. 4 – TEM image (a: catalyst-1, b: catalyst-2), HRTEM image (c: catalyst-1, d: catalyst-2).

surface of N,S-rGO but also prevented restacking of graphene layers resulting into a greater area of graphene for a higher dispersion of CdS particles on the surface of N,S-rGO.

HRTEM micrograph of catalysts-1 to 2 also shows that CdS particles are present in crystalline in nature and calculated d-values from lattice fringes well matched with the XRD results for each catalyst. The values confirmed that the CdS has a hcp structure. It is also observed that CdS particles are dispersed over the support rGO or doped rGO. Such dispersion may lead to the development of a chemical interaction between the interface of CdS and the support. The heterojunction thus formed will provide a pathway for the rapid movement of photoinduced e^- from the conduction band of CdS to the support for transfer to the solid-liquid interface for the reaction. In other words, the chemical interaction will reduce the possibility of recombination of holes and electrons.

Selected area electron diffraction patterns (SAED) of catalysts are presented in Fig. 5. It is seen that each catalyst shows a ring pattern thereby implying that CdS in catalysts were polycrystalline in nature. The interplanar spacings of each catalyst were calculated by using Image J software and corresponding d-values are marked against each ring for catalysts-1 and 2. These calculated d-values well-matched with values of XRD analysis. It is important to note that no cubic phase of CdS, which is less active [45], was detected in the as-synthesized catalysts.

Raman spectroscopy

Raman spectroscopy of prepared samples was performed to investigate defects in graphene and to identify layers of graphene. The Raman spectra of GO, N,S-rGO and MWCNT incorporated N,S-rGO are shown in Fig. 6. Each sample had two bands G and D. The D band originates due to the presence of disorders viz, lattice disorder, edge defects, defects due to functionalization of graphene. While G band represents the first-order Raman band of six carbon atoms sp^2 hybridised E_{2g} mode of graphene [47,48]. Previously, authors [49,50] have explained that D band to G band intensity ratio (I_D/I_G) represents the degree of defects in the graphene. Intensity ratio (I_D/I_G) for each sample is calculated and are presented in Fig. 8. Intensity ratio (I_D/I_G) of prepared samples follow the order MWCNT-N,S-rGO (1.23) > N,S-rGO (1.13) > GO (0.94). The value is higher in N,S-rGO compared to GO meaning that N, S-rGO had more disorder than GO due to the doping of N and S atom

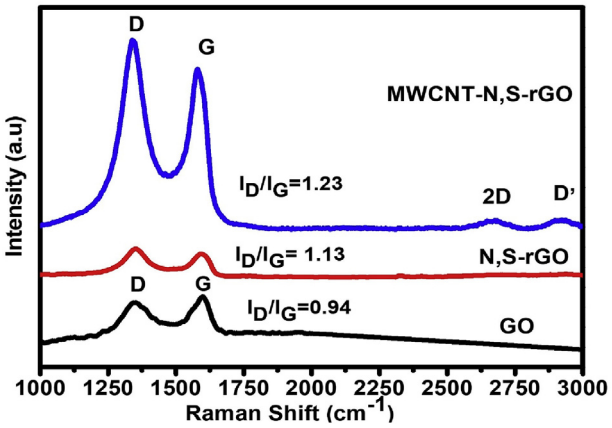

Fig. 6 – Raman spectra of GO, N, S-rGO and MWCNT-N, S-rGO.

in GO. In comparison to N,S-rGO, MWCNT incorporated N,S-rGO exhibited a higher degree of disorder. It is further observed that the second order Raman bands 2D and D' appeared at 2680 and 2924 cm^{-1}, respectively, in MWCNT incorporated N,S-rGO. These two bands reveal the presence of single-layer graphene and multiple layer graphene [51]. A similar observation is also reported by the literature [48,52]. Hence, this result also confirms that incorporation of MWCNT into N,S-rGO had prevented the restacking of graphene layers.

BET surface area

The Brunauer-Emmett-Teller (BET)surface area of catalysts was measured by N_2-adsorption technique. The surface area of catalyst 1 (CdS–N,S-r GO) was 26.6 m^2/g whereas that of catalyst 2 (CdS-MWCNT- N,S-r GO) was 43.0 m^2/g. The observed increase in the area in catalyst-2 may be attributed to two reasons firstly, the intercalation of MWCNT between the layers of N,S-rGO reduced the restacking of N,S-rGO layers and thus the increase in the area of the graphene sheet. Secondly, MWCNT itself which is composed of several layers of graphene sheet had its own surface area contributing to the total area.

Diffuse reflectance spectroscopy

Fig. 7(a) shows the DRS spectra of catalysts. The absorption edge of both the catalysts begins at a wavelength of 560 nm. It is also observed that the electronic transition of each catalyst

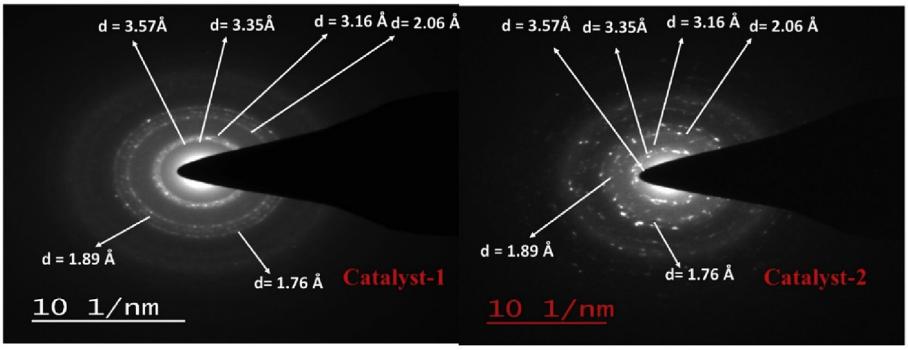

Fig. 5 – Selected Area Electron Diffraction (SAED) patterns of catalysts 1 and 2.

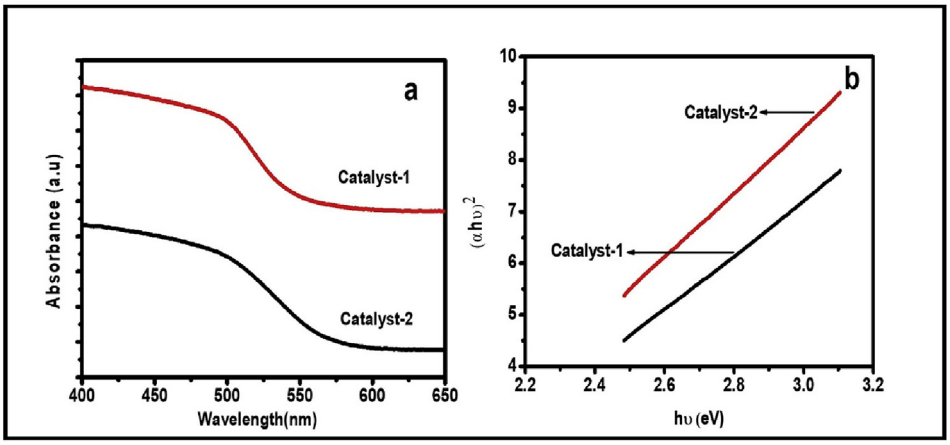

Fig. 7 – UV–Vis diffuse reflectance spectra (a: catalyst-1 and catalyst-2), Tauc plot (b: catalyst-1 and catalyst-2).

takes place in the visible region (560- 500 nm). It is also observed that catalyst-2 which was CdS supported on the surface of MWCNT-N,S-rGO shows higher absorption of light than catalyst-1. It is because of the introduction of MWCNT (in catalyst 2) provides surface electric charge on CdS. It is possible to have π to π^* transitions in MWCNT. Peng et al. [33] have also attributed the phenomena of the surface electric charge developed on CdS to the π to π^* transition of MWCNT. Furthermore, $n \rightarrow \pi^*$ electronic transitions also take place between n orbital of CdS and MWCNT.

Direct band gaps of catalysts were calculated by the linear extrapolation of the Tauc plot (Fig. 7(b)) and reported in Table 4. It is observed that both the catalysts had a band gap lower than the reported value (2.4 eV) of bare CdS. It may be explained that the interaction of CdS with rGO has resulted into Cd–S–C bond formation and created localized states in the band gap region of CdS and resulted into a narrowing of the effective band gap. This effect is higher in catalyst-2 because of the presence of MWCNT with N,S-rGO. The narrowing of the band gap enhances the absorption of light and increases the quantum efficiency of the catalyst. Earlier many authors have also reported that surface localized states may narrow the band gap of the catalyst [53–56]. Further, the phenomena have taken place to a greater extent in catalysts-2 when MWCNT was also incorporated in addition to rGO.

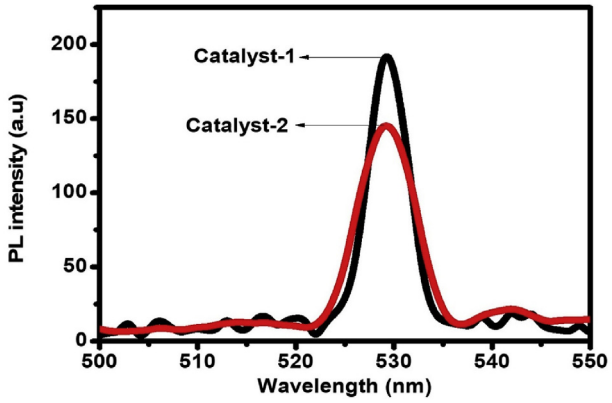

Fig. 8 – Photoluminescence spectra of catalyst-1 and catalyst-2.

Photoluminescence spectroscopy

Photoluminescence (PL) spectroscopy of catalysts was carried out to investigate the charge recombination behaviour of catalysts. The spectra are reported in Fig. 8. It is observed from the figure that the emission peak of each catalyst appeared at a wavelength 530 nm which is attributed to the band to band transition in the CdS. In comparison to catalysts-1, catalysts-2 which had MWCNT incorporated N,S-rGO showed lower PL intensity. It means a lower recombination rate of photoinduced electrons and holes. Literature [57,58] reports that incorporation of MWCNT with semiconductor materials capture the electrons from the surface of semiconductors and separate the photogenerated electrons and holes. A similar observation has been reported for rGO also [59]. Therefore, a synergistic effect of both rGO and MWCNT in separating electron-hole pair is observed in catalyst-2 and thereby reduction PL intensity and facilitating more electron available for reduction and enhanced activity of catalyst 2.

X-ray photoelectron spectroscopy

X-ray photoelectron spectroscopy of N, S-rGO, MWCNT-N,S-rGO and catalysts were carried out to determine the presence of elements and their chemical oxidation states in synthesized materials. The XPS peaks were de-convoluted by applying the Lorentzian Gaussian fitting. The N 1s XPS spectra of NS-rGO, MWCNT-N,S-rGO, catalysts-1 to 2 are shown in Fig. 9. Miscellaneous N species, especially pyrrolic, pyridinic, and graphitic are observed. Peak positions are reported in Table 5. Peaks centred at 401.1, 399.9, 399.1 eV correspond to graphitic N, pyrrolic N, pyridinic N, respectively [52,60–62]. The S 2p spectra of N,S-rGO and MWCNT-N,S-rGO had a single doublet and are shown in Fig. 10. Peak positions are presented in Table 6. The two peaks of N,S-rGO at 163.1 eV, 164.2eV are attributed to $2p_{3/2}$ and $2p_{1/2}$ of S in thiophene (C–S–C) groups, respectively, which are attached to the basal plane of graphene. Xu et al. [63] have also explained the appearance of this

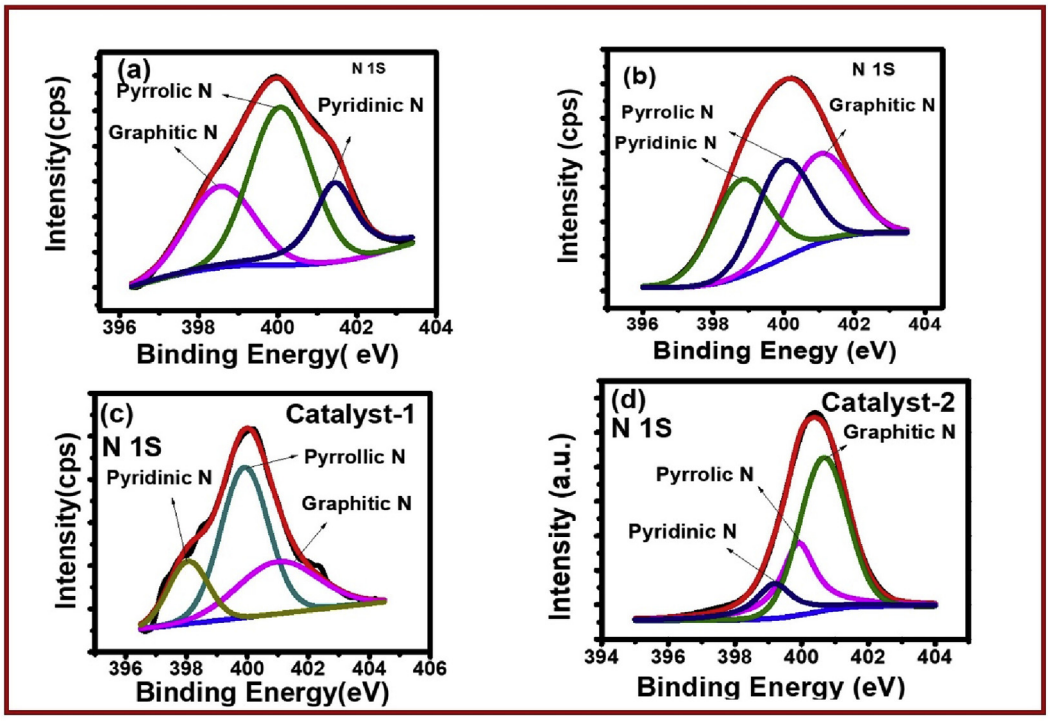

Fig. 9 – N 1S XPS spectra (a: N,S-rGO), b: MWCNT-N,S-rGO, c: catalyst-1, d: catalyst-2).

group. On comparison of S 2p spectra of MWCNT-N,S-rGO with that of N,S-rGO, it is observed that the binding energies of $2p_{3/2}$ and $2p_{1/2}$ peaks shift toward positive values. It indicates a chemical interaction between MWCNT and N,S-rGO. The S 2p spectra of catalysts −1 to 2 are also shown in Fig. 10. Both catalysts had two resolved doublets. The peak positions were calculated and are presented in Table 6. The first doublet has been assigned to S^{2-} of CdS. The second doublet is ascribed to S^{2-} of C–S–C or C–S. Peak positions of S^{2-} of CdS of each catalyst which correspond to $2p_{3/2}$ and $2p_{1/2}$ matched with values (161.1 and 162.2 eV) reported in the literature [64,65] with a noticeable positive shift. The shift in binding energy is attributed to a chemical interaction between CdS and N,S-rGO or MWCNT-N,S-rGO at the interface. The interaction is considered to be between n orbitals of S in CdS and π orbital of C of graphene. In our earlier communication [35] we have reported that the catalyst prepared by a high-temperature solid-gas reaction had promoted such interaction. In the present study also catalysts were prepared following the same protocol and positive shifts are observed. Further, the shift is more in catalyst-2 where MWCN T was also incorporated indicating a greater chemical interaction due to the presence of MWCNT because of the presence of π-π conjugation in MWCNT. Therefore, it is concluded that the presence of MWCNT in N,S-rGO has strengthened the above-stated surface interaction and promoting to a greater extent the formation of a heterojunction between CdS and MWCNT-N,S-rGO, which is considered to promote the transfer of electrons from the conduction band of CdS to the support. Since this interaction has taken place to a greater extent in catalyst-2, it had a higher activity compared to the catalyst-1.

Table 5 – XPS N 1s peaks of samples.

Samples	The position of N 1s peak (eV)		
	Pyridinic N	Pyrrolic N	Graphitic N
NS-rGO	399.1	399.9	401.1
MWCNT-N,S-rGO	399.3	399.9	401.1
Catalyst −1	399.5	400.3	401.2
Catalyst-2	399.6	400.1	401.2

The XPS spectrum (Fig. 11) of Cd^{2+} for both catalysts showed a doublet and binding energies are presented in Table 6. On comparison with standard values i.e, 404.85 and 411.73 eV, respectively [66], positive shifts are observed. Further, as compared above for S^{2-}, the shift is more when MWCNT was incorporated in (catalyst-2). Arvind and Sinha [35] have explained that the chemical interaction between C of rGO and S of CdS leads to polarization of charges and positive shift in the binding energy of Cd^{2+}. Since, the positive shift was higher in catalyst-2, therefore, as concluded earlier, a greater surface interaction existed in catalyst-2 due to the incorporation of MWCNT.

Electrical impedance spectroscopy

Electrical impedance spectroscopy (EIS) was carried out to measure charge transfer resistances of supports viz, N,S-rGO, MWCNT-N,S-rGO and catalysts. Experiments were carried out at the room temperature. Nyquist plots of, NS-rGO and MWCNT-N,S-rGO are shown in Fig. 12(a). Nyquist plots were used to get the equivalent circuit models (Randel Cell) shown in the inset of Fig. 12(a). Values of the circuit elements, viz, the charge transfer resistance (R_1), solution resistance (R_s) and the

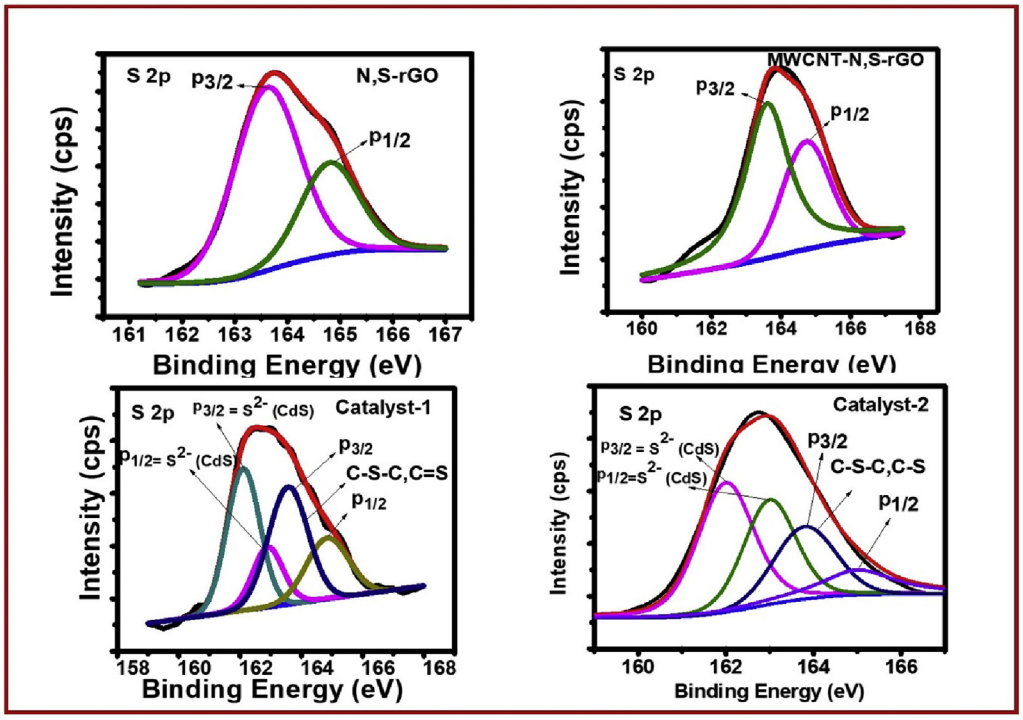

Fig. 10 – S 2p XPS spectra of N-rGO, MWCNT-N,S-rGO and catalysts 1 and 2.

double layer capacitance (C_1), were determined using the software (ZSimpWin 3.21). The calculated values are reported in Table 7. It is observed that MWCNT intercalated N,S-rGO had a lower charge transfer resistance and therefore higher conductivity than N, S-rGO due to the presence of MWCNT. It may be because MWCNT has a higher π-π electronic conjugation than N,S-rGO. N,S-rGO which was prepared by doping of N and S into graphite oxide (GO) may have resulted in disruption the π-π electronic conjugation.

The Nyquist plots for the catalysts are shown in Fig. 12(b). Plots are semi-circle for catalysts also. Therefore, the simplified Randle equivalent circuit, as shown above, was fitted and the results are reported in Table 7. It is observed that catalyst −2 which was CdS supported on the surface of MWCNT-N,S-rGO had a significantly lower charge transfer resistance (145 Ω) than catalysts 1- (312 Ω) because of delocalization of π-π electrons of MWCNT. The Charge transfer resistance follows the order catalyst-1 > catalyst-2. The activity followed the reverse order as catalyst 2 > catalyst 1. Thus it may be concluded that the high activity of catalyst 2 was due to the quick transfer of photogenerated electrons from the conduction band of CdS to the solid-liquid interface to mediate the reduction of water to hydrogen. Therefore, the addition of MWCNT not only had increased the surface area

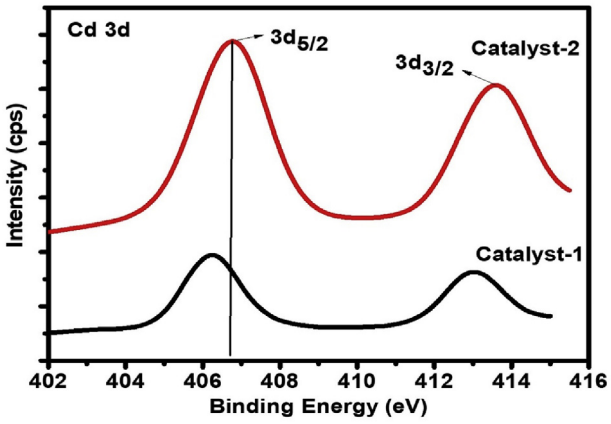

Fig. 11 – Cd 3d XPS spectra of catalysts 1- and 2.

Table 6 – Results of XPS S 2p and Cd 3d of peaks of samples.

Samples	Sulphur				Cadmium	
	First doublet		Second doublet		3d orbital	
	$p_{3/2}$ (eV)	$p_{1/2}$ (eV)	$p_{3/2}$ (eV)	$p_{1/2}$ (eV)	$3d_{3/2}$ (eV)	$3d_{5/2}$ (eV)
N,S-rGO	-	-	163.1	164.2	-	-
MWCNT-N,S-rGO	–	–	163.6	164.7	–	–
Catalyst-1	161.8	162.9	163.7	164.9	413.0	406.1
Catalyst-2	162.0	163.1	163.8	165.0	413.6	406.7

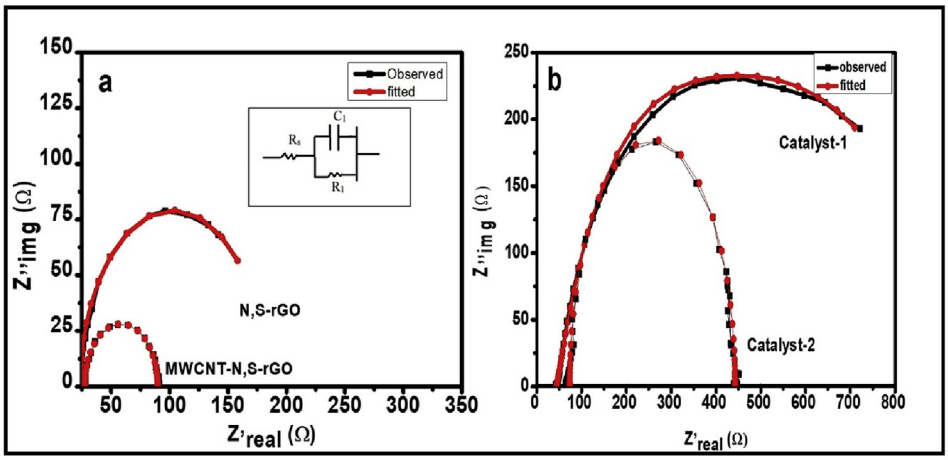

Fig. 12 – Nyquist plots (a: N,S-rGO and MWCNT-N,S-rGO) and (b: catalyst-1 and catalyst-2) at 100 mV (rms).

and prevented the re-stacking of rGO but also improved the charge transfer properties.

It is also observed that the double layer capacitances of both N,S-rGO and MWCNT-N, S -rGO are very low indicating negligible charge accumulation at the interface and faster electron transfer. However, the incorporation of CdS with either N,S-rGO or MWCNT-N,S-rGO results into increase of double layer capacitance to about 73 and 66 μF for catalyst-1 and catalyst-2, respectively. This enhancement is attributed to the presence of high dielectric CdS semiconductor in both the catalysts. Further, a lower value for catalyst 2 supports the conclusion drawn above that the presence of MWCNT in N, S-rGO has resulted into a faster transfer of electrons.

Table 7 – Fitted parameters of Nyquist plot using Randle equivalent circuit model.

Sample	R_S (Ω)	R1(Ω)	C1 (μF)
NS-rGO	23.62	158	0.80
MWCNT-N,S-rGO	25.22	95	0.75
Catalyst-1	28.2	312	76.36
Catalyst-2	27.1	145	66.23

Mott. Schottky analysis

Mott. Schottky analyses of catalysts were carried out to estimate flat band potentials and charge carrier densities along with nature of semiconductivity. Fig. 13 represents M.S plots of synthesized catalysts. Following equation was used to calculate the values of flat band potential and charge carrier densities.

$$\frac{1}{C^2} = \frac{2}{N_d A^2 q\varepsilon\varepsilon_0}\left[V - V_{fb} - \frac{kT}{q}\right] \quad (7)$$

where, N_d represents the charge carrier densities, C is the space charge capacitance q is the electronic charge (1.602×10^{-19} C), ε is the dielectric constant of catalyst (9), ε_0 is the permittivity in free space (8.85×10^{-12} F/m), V_{fb} is the flat band, V is the applied potential, potential, k is the Boltzmann constant, and T is temperature in Kelvin scale. The potential V was converted to NHE from Ag/AgCl reference values by using equation (8).

$$V_{fb}\,(NHE) = V_{fb(vs\ Ag/Agcl)} + 0.197 + .059\ pH \quad (8)$$

Positive slopes of M.S plots confirmed that each catalyst had n-type semiconductivity and hence the majority charge carriers were electrons. Charge carrier densities and Flat band

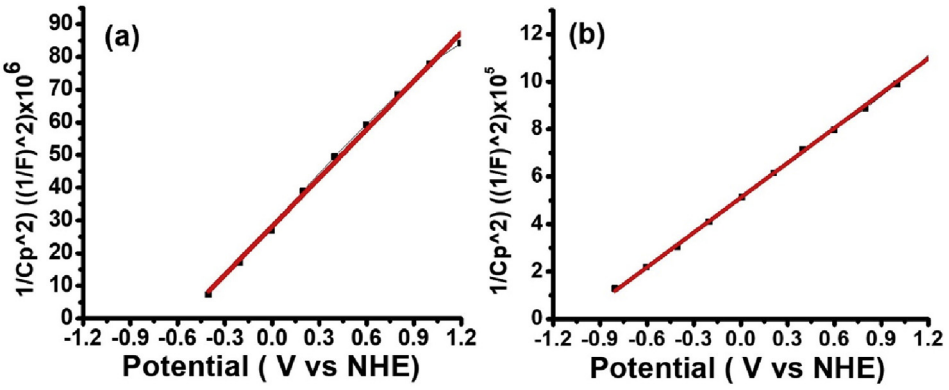

Fig. 13 – Mott. Schottky plots (a: catalyst-1) and (b: catalyst-2) at 100 mV (rms).

Table 8 – Results of Mott. Schottky analysis.

Catalysts	Flat band potential V vs NHE	Carrier density (N_d) (cm^{-3})
Catalyst-1	−0.95	4.471×10^{23}
Catalyst-2	−1.0	3.33×10^{24}

potential (V_{fb}) were calculated from the slopes and intercepts of M.S plots (Table 8). It is also observed that catalyst −2 possesses 10 folds higher carrier densities than catalyst-1. Literature reports [67–69] that a chemical interaction at the solid-solid interface between the semiconductors and supports increased charge carrier densities. Therefore, the present observation is in line with our earlier conclusion on the basis of XPS, that the extent of chemical interaction between CdS and supports was more when MWCNT was incorporated in N,S- rGO. The flat band potential is also higher in catalyst 2. It is known that the flat band potential results into band bending of a semiconductor which causes separation of photoinduced electrons and holes. Thus, a greater band bending in catalyst 2 may have also contributed towards a higher activity of catalyst 2.

Conclusions

CdS supported on MWCNT-N,S-rGO synthesized by a high-temperature gas-solid reaction showed the formation of a heterojunction at the solid-solid interface. The chemical interaction leading to the formation of the heterojunction is considered to be due to a high-temperature synthesis route. The interaction is found to be more when MWCNT was incorporated into the N,S-rGO. Formation of the heterojunction at the solid-solid interface promoted the transfer of electrons from the conduction band of CdS to the support doped r GO. The incorporation of MWCNT also prevented restacking of graphene layers and thus provided a high area for better dispersion of CdS. Furthermore, incorporation of MWCNT also results in the enhancement of light absorption, charge carrier density and the flat band potentials. The combined effect of the above observations has resulted into a higher rate of photoinduced electron transfer from the CdS to the doped rGO. MWCNT also increased the electrical conductivity of the catalyst due to the presence of π-π conjugation and therefore, higher mobility of electrons to the solid-liquid interface to carry out the reduction of water. Thus, it is concluded that the incorporation of MWCNT to CdS supported on N,S- rGO makes more number of electrons with higher mobility available for the reduction of water. The Catalyst was found to be stable in repeated runs.

Acknowledgements

This work was supported in the form of teaching assistantship provided by the Ministry of Human Resource Development, Government of India.

REFERENCES

[1] Wang J, Wang P, Wang C, Ao Y. In-situ synthesis of well dispersed CoP nanoparticles modified CdS nanorods composite with boosted performance for photocatalytic hydrogen evolution. Int J Hydrogen Energy 2018;43:14934–43.
[2] Wang J, Wang Z, Qu P, Xu Q, Zheng J, Jia S, et al. A 2D/1D TiO_2 nanosheet/CdS nanorods heterostructure with enhanced photocatalytic water splitting performance for H_2 evolution. Int J Hydrogen Energy 2018;43:7388–96.
[3] Qi L, Yu J, Jaroniec M. Preparation and enhanced visible-light photocatalytic H 2-production activity of CdS-sensitized Pt/TiO_2 nanosheets with exposed (001) facets. Phys Chem Chem Phys 2011;13:8915–23.
[4] Xin G, Yu B, Xia Y, Hu T, Liu L, Li C. Highly efficient deposition method of platinum over CdS for H_2 evolution under visible light. J Phys Chem C 2014;118:21928–34.
[5] Wang Y, Wang Y, Xu R. Photochemical deposition of Pt on CdS for H_2 evolution from water: markedly enhanced activity by controlling Pt reduction environment. J Phys Chem C 2013;117:783–90.
[6] Yu H, Chen F, Chen F, Wang X. In situ self-transformation synthesis of g-C_3N_4-modified CdS heterostructure with enhanced photocatalytic activity. Appl Surf Sci 2015;358:385–92.
[7] Tonda S, Kumar S, Gawli Y, Bhardwaj M, Ogale S. g-C_3N_4 (2D)/CdS (1D)/rGO (2D) dual-interface nano-composite for excellent and stable visible light photocatalytic hydrogen generation. Int J Hydrogen Energy 2017;42:5971–84.
[8] Ranjan R, Kumar M, Sinha A. Development and characterization of rGO supported CdSMoS2 photoelectrochemical catalyst for splitting water by visible light. Int J Hydrogen Energy 2019;44:16176–89.
[9] Shen R, Jiang C, Xiang Q, Xie J, Li X. Surface and interface engineering of hierarchical photocatalysts. Appl Surf Sci 2019;471:43–87.
[10] Bellamkonda S, Rao GR. Nanojunction-mediated visible light photocatalytic enhancement in heterostructured ternary BiOCl/CdS/g-C_3N_4 nanocomposites. Catal Today 2019;321:18–25.
[11] Li X, Yu J, Wageh S, Al-Ghamdi AA, Xie J. Graphene in photocatalysis: a review. Small 2016;12:6640–96.
[12] Fajrina N, Tahir M. A critical review in strategies to improve photocatalytic water splitting towards hydrogen production. Int J Hydrogen Energy 2019;44:540–77.
[13] Low J, Cao S, Yu J, Wageh S. Two-dimensional layered composite photocatalysts. Chem Commun 2014;50:10768–77.
[14] Shinde SS, Sami A, Lee JH. Nitrogen-and Phosphorus-doped nanoporous graphene/graphitic carbon nitride hybrids as efficient electrocatalysts for hydrogen evolution. ChemCatChem 2015;7:3873–80.
[15] Qu K, Zheng Y, Zhang X, Davey K, Dai S, Qiao SZ. Promotion of electrocatalytic hydrogen evolution reaction on nitrogen-doped carbon nanosheets with secondary heteroatoms. ACS Nano 2017;11:7293–300.
[16] Putri LK, Ng B-J, Ong W-J, Lee HW, Chang WS, Chai S-P. Heteroatom nitrogen-and boron-doping as a facile strategy to improve photocatalytic activity of standalone reduced graphene oxide in hydrogen evolution. ACS Appl Mater Interfaces 2017;9:4558–69.
[17] Putri LK, Ong W-J, Chang WS, Chai S-P. Heteroatom doped graphene in photocatalysis: a review. Appl Surf Sci 2015;358:2–14.

[18] Huang L, Cao Y, Diao D. N-doped graphene sheets induced high electrochemical activity in carbon film. Appl Surf Sci 2019;470:205–11.
[19] Li X, Shen R, Ma S, Chen X, Xie J. Graphene-based heterojunction photocatalysts. Appl Surf Sci 2018;430:53–107.
[20] Deng D, Pan X, Yu L, Cui Y, Jiang Y, Qi J, et al. Toward N-doped graphene via solvothermal synthesis. Chem Mater 2011;23:1188–93.
[21] Jia L, Wang D-H, Huang Y-X, Xu A-W, Yu H-Q. Highly durable N-doped graphene/CdS nanocomposites with enhanced photocatalytic hydrogen evolution from water under visible light irradiation. J Phys Chem C 2011;115:11466–73.
[22] Kong L, Wang J, Ma F, Sun M, Quan J. Graphitic carbon nitride nanostructures: Catalysis. Appl Mater Today 2019;16:388–424.
[23] Han B, Liu S, Tang Z-R, Xu Y-J. Electrostatic self-assembly of CdS nanowires-nitrogen doped graphene nanocomposites for enhanced visible light photocatalysis. J Energy Chem 2015;24:145–56.
[24] Han W, Chen L, Song W, Wang S, Fan X, Li Y, et al. Synthesis of nitrogen and sulfur co-doped reduced graphene oxide as efficient metal-free cocatalyst for the photo-activity enhancement of CdS. Appl Catal B Environ 2018;236:212–21.
[25] Kotal M, Bhowmick AK. Multifunctional hybrid materials based on carbon nanotube chemically bonded to reduced graphene oxide. J Phys Chem C 2013;117:25865–75.
[26] Novaes FD, Rurali R, Ordejón P. Electronic transport between graphene layers covalently connected by carbon nanotubes. ACS Nano 2010;4:7596–602.
[27] Yu D, Dai L. Self-assembled graphene/carbon nanotube hybrid films for supercapacitors. J Phys Chem Lett 2009;1:467–70.
[28] Wang Y, Wu Y, Huang Y, Zhang F, Yang X, Ma Y, et al. Preventing graphene sheets from restacking for high-capacitance performance. J Phys Chem C 2011;115:23192–7.
[29] Zhang N, Zhang Y, Yang M-Q, Tang Z-R, Xu Y-J. A critical and benchmark comparison on graphene-, carbon nanotube-, and fullerene-semiconductor nanocomposites as visible light photocatalysts for selective oxidation. J Catal 2013;299:210–21.
[30] Weng B, Liu S, Zhang N, Tang Z-R, Xu Y-J. A simple yet efficient visible-light-driven CdS nanowires-carbon nanotube 1D–1D nanocomposite photocatalyst. J Catal 2014;309:146–55.
[31] Zhang W, Chen X, Zhang J, Tuo C, Ji L, Li H, et al. Exposure of active edge structure for electrochemical H_2 evolution from VS_2/MWCNTs hybrid catalysts. Int J Hydrogen Energy 2018;43:22949–54.
[32] Robel I, Bunker BA, Kamat PV. Single-walled carbon nanotube–CdS nanocomposites as light-harvesting assemblies: photoinduced charge-transfer interactions. Adv Mater 2005;17:2458–63.
[33] Peng T, Zeng P, Ke D, Liu X, Zhang X. Hydrothermal preparation of multiwalled carbon nanotubes (MWCNTs)/CdS nanocomposite and its efficient photocatalytic hydrogen production under visible light irradiation. Energy Fuels 2011;25:2203–10.
[34] Shen L, Zhang X, Li H, Yuan C, Cao G. Design and tailoring of a three-dimensional TiO2–graphene–carbon nanotube nanocomposite for fast lithium storage. J Phys Chem Lett 2011;2:3096–101.
[35] Singh A, Sinha A. Active CdS/rGO photocatalyst by a high temperature gas-solid reaction for hydrogen production by splitting of water. Appl Surf Sci 2018;430:184–97.
[36] Acik M, Lee G, Mattevi C, Pirkle A, Wallace RM, Chhowalla M, et al. The role of oxygen during thermal reduction of graphene oxide studied by infrared absorption spectroscopy. J Phys Chem C 2011;115:19761–81.
[37] Keuleers R, Desseyn H, Rousseau B, Van Alsenoy C. Vibrational analysis of urea. J Phys Chem A 1999;103:4621–30.
[38] Du D, Li P, Ouyang J. Nitrogen-doped reduced graphene oxide prepared by simultaneous thermal reduction and nitrogen doping of graphene oxide in air and its application as an electrocatalyst. ACS Appl Mater Interfaces 2015;7:26952–8.
[39] Yang G, Wan X, Su Y, Zeng X, Tang J. Acidophilic S-doped carbon quantum dots derived from cellulose fibers and their fluorescence sensing performance for metal ions in an extremely strong acid environment. J Mater Chem 2016;4:12841–9.
[40] Khan ZR, Zulfequar M, Khan MS. Chemical synthesis of CdS nanoparticles and their optical and dielectric studies. J Mater Sci 2011;46:5412–6.
[41] Yogamalar NR, Sadhanandam K, Bose AC, Jayavel R. Quantum confined CdS inclusion in graphene oxide for improved electrical conductivity and facile charge transfer in hetero-junction solar cell. RSC Adv 2015;5:16856–69.
[42] Alam Z, Verma B, Sinha ASK. Creation of heterojunction in CdS supported on N, S-rGO for efficient charge separation and photo-reduction of water to hydrogen. [Revised submitted].
[43] Son Y-R, Park S-J. Green preparation and characterization of graphene oxide/carbon nanotubes-loaded carboxymethyl cellulose nanocomposites. Sci Rep 2018;8.
[44] Woo S, Kim Y-R, Chung TD, Piao Y, Kim H. Synthesis of a graphene–carbon nanotube composite and its electrochemical sensing of hydrogen peroxide. Electrochim Acta 2012;59:509–14.
[45] Zhang J, Wageh S, Al-Ghamdi A, Yu J. New understanding on the different photocatalytic activity of wurtzite and zinc-blende CdS. Appl Catal B Environ 2016;192:101–7.
[46] Barpuzary D, Khan Z, Vinothkumar N, De M, Qureshi M. Hierarchically grown urchinlike CdS@ ZnO and CdS@ $Al2O_3$ heteroarrays for efficient visible-light-driven photocatalytic hydrogen generation. J Phys Chem C 2011;116:150–6.
[47] Guo L, Ren L, Wan L, Li J. Heterogeneous carbon/N-doped reduced graphene oxide wrapping LiMn0. $8Fe_{0.2}PO_4$ composite for higher performance of lithium ion batteries. Appl Surf Sci 2019;476:513–20.
[48] Ferrari AC, Meyer J, Scardaci V, Casiraghi C, Lazzeri M, Mauri F, et al. Raman spectrum of graphene and graphene layers. Phys Rev Lett 2006;97:187401.
[49] Eckmann A, Felten A, Mishchenko A, Britnell L, Krupke R, Novoselov KS, et al. Probing the nature of defects in graphene by Raman spectroscopy. Nano Lett 2012;12:3925–30.
[50] Ferrari AC, Basko DM. Raman spectroscopy as a versatile tool for studying the properties of graphene. Nat Nanotechnol 2013;8:235.
[51] Graf D, Molitor F, Ensslin K, Stampfer C, Jungen A, Hierold C, et al. Spatially resolved Raman spectroscopy of single-and few-layer graphene. Nano Lett 2007;7:238–42.
[52] Zhang J, Li C, Peng Z, Liu Y, Zhang J, Liu Z, et al. 3D free-standing nitrogen-doped reduced graphene oxide aerogel as anode material for sodium ion batteries with enhanced sodium storage. Sci Rep 2017;7:4886.
[53] Zhang X-Y, Li H-P, Cui X-L, Lin Y. Graphene/TiO_2 nanocomposites: synthesis, characterization and application in hydrogen evolution from water photocatalytic splitting. J Mater Chem 2010;20:2801–6.
[54] Ye A, Fan W, Zhang Q, Deng W, Wang Y. CdS–graphene and CdS–CNT nanocomposites as visible-light photocatalysts for hydrogen evolution and organic dye degradation. Catal Sci Technol 2012;2:969–78.

[55] Lee JS, You KH, Park CB. Highly photoactive, low bandgap TiO_2 nanoparticles wrapped by graphene. Adv Mater 2012;24:1084–8.
[56] Xing Z, Zong X, Zhu Y, Chen Z, Bai Y, Wang L. A nanohybrid of CdTe@ CdS nanocrystals and titania nanosheets with p–n nanojunctions for improved visible light-driven hydrogen production. Catal Today 2016;264:229–35.
[57] Delekar SD, Dhodamani AG, More KV, Dongale TD, Kamat RK, Acquah SF, et al. Structural and optical properties of nanocrystalline TiO_2 with multiwalled carbon nanotubes and its photovoltaic studies using Ru (II) sensitizers. ACS Omega 2018;3:2743–56.
[58] Woan K, Pyrgiotakis G, Sigmund W. Photocatalytic carbon-nanotube–2 composites. Adv Mater 2009;21:2233–9.
[59] Li Q, Guo B, Yu J, Ran J, Zhang B, Yan H, et al. Highly efficient visible-light-driven photocatalytic hydrogen production of CdS-cluster-decorated graphene nanosheets. J Am Chem Soc 2011;133:10878–84.
[60] Li Z, Gao Q, Zhang H, Tian W, Tan Y, Qian W, et al. Low content Pt nanoparticles anchored on N-doped reduced graphene oxide with high and stable electrocatalytic activity for oxygen reduction reaction. Sci Rep 2017;7:43352.
[61] Lu H, Huang Y, Yan J, Fan W, Liu T. Nitrogen-doped graphene/carbon nanotube/Co 3 O 4 hybrids: one-step synthesis and superior electrocatalytic activity for the oxygen reduction reaction. RSC Adv 2015;5:94615–22.
[62] Kong L, Mu X, Fan X, Li R, Zhang Y, Song P, et al. Site-selected N vacancy of g-C3N_4 for photocatalysis and physical mechanism. Appl Mater Today 2018;13:329–38.
[63] Xu X, Chu H, Zhang Z, Dong P, Baines R, Ajayan PM, et al. Integrated energy aerogel of N, S-rGO/WSe2/NiFe-LDH for both energy conversion and storage. ACS Appl Mater Interfaces 2017;9:32756–66.
[64] Hong S, Kumar DP, Reddy DA, Choi J, Kim TK. Excellent photocatalytic hydrogen production over CdS nanorods via using noble metal-free copper molybdenum sulfide (Cu_2MoS_4) nanosheets as co-catalysts. Appl Surf Sci 2017;396:421–9.
[65] Zhang J, Wang Y, Jin J, Zhang J, Lin Z, Huang F, et al. Efficient visible-light photocatalytic hydrogen evolution and enhanced photostability of core/shell CdS/g-C_3N_4 nanowires. ACS Appl Mater Interfaces 2013;5:10317–24.
[66] Lee H, Reddy DA, Kim Y, Chun SY, Ma R, Kumar DP, et al. Drastic improvement of 1D-CdS solar-driven photocatalytic hydrogen evolution rate by integrating with NiFe layered double Hydroxide nanosheets synthesized by liquid-phase pulsed-laser ablation. ACS Sustainable Chem Eng 2018;6:16734–43.
[67] Li G, Wang T, Zhu Y, Zhang S, Mao C, Wu J, et al. Preparation and photoelectrochemical performance of Ag/graphene/TiO_2 composite film. Appl Surf Sci 2011;257:6568–72.
[68] Ranjan R, Sinha A. Optimizations of r GO supported CdS photo-electrocatalyst for dissociation of water. Int J Hydrogen Energy 2019;44:5955–69.
[69] Ranjan R, Kumar M, Sinha A. CdS supported on electrochemically reduced rGO for photo reduction of water to hydrogen. Int J Hydrogen Energy 2019;44:10573–84.